Development of Polarization Interferometer for Thomson Scattering Diagnostics in JT-60U

Takaki HATAE, John HOWARD[1)], Noboru EBIZUKA[2)*], Youich HIRANO[3)], Haruhisa KOGUCHI[3)], Shigeru KITAMURA, Takeshi SAKUMA, Takashi HAMANO

Fusion Research and Development Directorate, Japan Atomic Energy Agency, 801-1 Mukouyama, Naka, Ibaraki 311-0193, Japan

[1)]Plasma Research Laboratory, The Australian National University, Canberra ACT 0200, Australia

[2)]Department of physics, Konan University, 8-9-1 Okamoto, Higashi-Nada, Kobe, Hyogo 658-8501, Japan

[3)]National Institute of Advanced Industrial Science and Technology, 1-1-1 Umezono, Tsukuba, Ibaraki 305-8568, Japan

(Received: 1 September 2008 / Accepted: 7 January 2009)

A polarization interferometer based on the Fourier transform spectroscopy for the Thomson scattering diagnostics is being developed to evaluate the validity. At the first stage, a dual channel polarization interferometer utilizing a fixed-thickness birefringent plate is developed, and the target T_e and n_e ranges were < 1 keV and > $5\text{x}10^{18}$ m^{-3}, respectively. The electron temperature is successfully measured by the dual channel polarization interferometer in TPE-RX reversed field pinch machine, for the first time. The temperature of the polarization interferometer nearly agrees with that of a filter polychromator. At the second stage, we are developing a multichannel polarization interferometer employing a Wallaston prism to cover wider range of electron temperature. Interferograms of three kinds of monochromatic light sources are measured by the multichannel polarization interferometer, and those spectra are reconstructed by Fourier transform.

Keywords: Thomson scattering, Fourier transform spectroscopy, polarization interferometer, birefringent plate, Wollaston prism

1. Introduction

In the Thomson scattering diagnostics, grating spectrometers [1,2] or filter polychromators [3-5] have been widely used to analyze the scattered spectrum thus far. Although these are established methods, there are some disadvantages: the throughput is relatively small in the case of grating spectrometer, the transmissivity decreases when the polychromator has many wavelength channels. It is well known that Fourier transform spectrometers [6] offer some potential advantages over grating systems. Fourier transform spectroscopy is a measurement technique whereby spectra are collected based on measurements of the temporal coherence of a radiative source, using time-domain measurements of the electromagnetic radiation [7]. In general, the main advantages of the Fourier spectroscopy are as follows. (1) The Fourier transform spectrometer (i.e. interferometer to measure the temporal coherence) can use the optical system of the high throughput (Jacquinot advantage). (2) Since the Fourier transform spectrometer observes the whole wavelength area at the same time, the S/N ratio is improved (Fellgett advantage). More importantly, for this application, the method can be implemented in a simple, compact, and robust system. Furthermore, this method is suitable for an imaging measurement. Optical coherence techniques based on the Fourier spectroscopy have been successfully applied for plasma spectroscopy. In particular, high-throughput, wide field-of view polarization interferometers have been used for Doppler imaging of ion temperature in the H-1 heliac [8-10]. These modulated or static coherence imaging systems monitor the complex coherence (fringe visibility and phase) of an isolated spectral line at one or more optical delays. A method based on measurement of the optical coherence of scattered radiation at a fixed optical delay has also been proposed for incoherent Thomson scattering, recently [11]. However, there has been no experimental results applied Fourier transform spectroscopy to the Thomson scattering diagnostics, yet.

In this paper, we report progress in development of polarization interferometer for Thomson scattering in JT-60U. It is presented about the development of a dual channel polarization interferometer in Sec. 2. In Sec.3, the development and basic tests of multichannel polarization interferometer are presented. Finally, conclusions are listed in Sec. 4.

author's e-mail: hatae.takaki@jaea.go.jp

**present address:* Graduate School of Science, Nagoya University, Furo-cho, Chikusa-ku, Nagoya, Aichi 464-8602, Japan

2. Dual channel polarization interferometer

The polarization interferometer is composed of a birefringent plate of fixed optical delay sandwiched between polarizers [11]. When the monochromatic light source with limited divergence is observed using this interferometer, interference fringe appears in the infinity based on the Fresnel-Arago law. Thomson scattered radiation that traverses the first polarizer is incident on a birefringent plate whose fast axis is oriented at 45° to the polarization direction. The plate splits the incident scattered scalar wave component, relatively delaying nominally equal amplitude components by time τ before they recombine at a final polarizer and are focused on to a detector. The orthogonally polarized outputs at the final polarizing splitter form complementary, or antiphase interferometric images of the input radiation. By suitably choosing the optical delay, these independent outputs provide sufficient information to determine both the electron temperature and density.

A schematic of the dual channel polarization interferometer for Thomson scattering diagnostics [12] is illustrated in Fig. 1. Scattered light is collected and introduced to the polarization interferometer through a fiber-optic bundle. This polarization interferometer consists of an objective lens as the fiber coupling optics, a band pass filter, polarizers, a birefringent plate which gives optical path delay, an imaging optics to detector, and dual detectors.

For radiation of centre frequency ν_0, the interferometer signal at either of the final polarizer ports is given by

$$S_{\pm} = \frac{I_0}{2}(1 \pm \zeta \cos\phi_0), \qquad (1)$$

where $\phi_0 = 2\pi\nu_0\tau_0 = 2\pi N$ is monochromatic birefringent phase delay, and τ_0, N are the center-frequency time delay and the order of interference, respectively [12]. The fringe visibility (fringe amplitude normalized to mean intensity) $\zeta = \zeta_I \zeta_T$ includes an instrumental component ζ_I due to the average of the birefringent plate delay over the angular extent of the source (analogous to familiar slit function for grating spectrometers) as well as the degradation ζ_T due to the finite source spectral width.

For a thermal distribution of T_e < 1keV, the fringe visibility associated with the Thomson scattered light takes the simple form

$$\zeta_T(\phi_0) = \exp[-\hat{\phi}_0^2 \sin^2(\theta/2) v_{th}^2] = \exp(-T_e/T_C), \qquad (2)$$

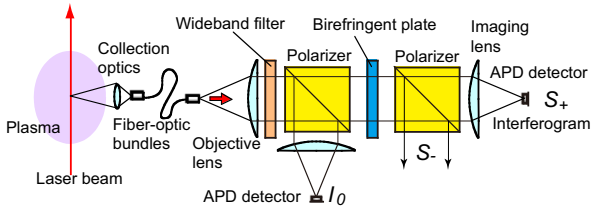

Fig.1 Schematic of the dual channel polarization interferometer.

where $\hat{\phi}_0, \theta$ are the group phase delay and the angle between the incident and scattered wavevectors, respectively. T_C is a 'characteristic temperature' set by the waveplate delay and the scattering angle

$$kT_C = \frac{1}{2} m_e c^2 \Big/ [\hat{\phi}_0 \sin(\theta/2)]^2. \qquad (3)$$

Optimum sensitivity to temperature variation is obtained when the optical delay is chosen such that $T_e \sim T_C$, or $\Delta\nu/\nu_0 \sim 1/N$, where $\Delta\nu/\nu_0$ is the Thomson spectral bandwidth [9].

For the low temperature (T_e < 1keV), the variation of fringe visibility with temperature is best measured by setting $\phi_0/2\pi = M/2$ where M represents an integer number of half waves. A quartz waveplate will be used as the

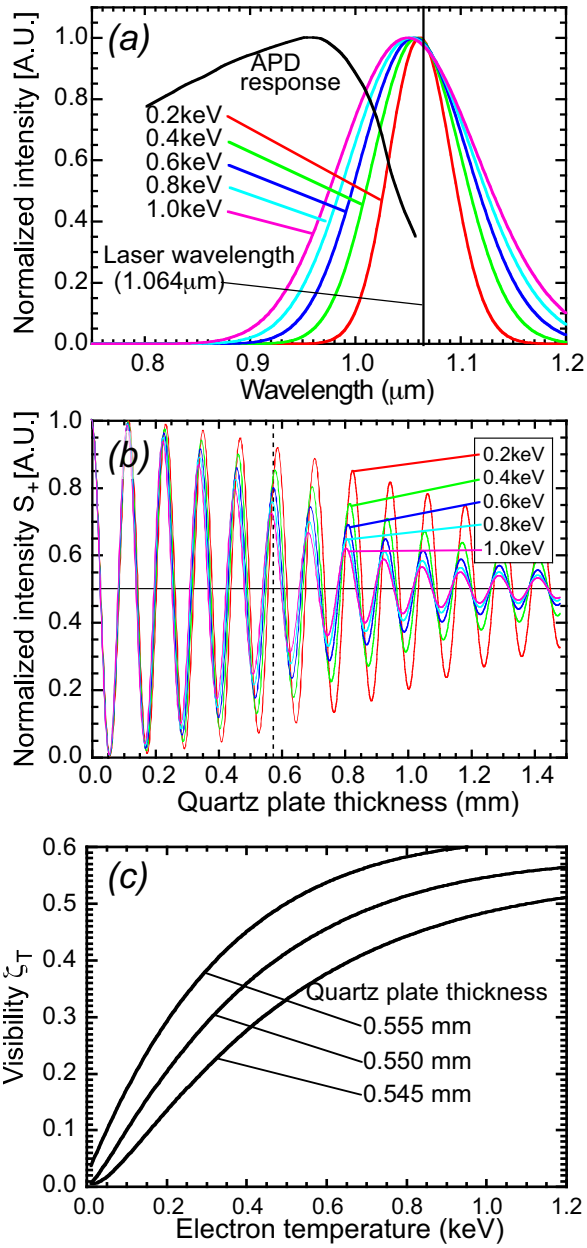

Fig.2 (a) Thomson scattered spectra and (b) their associated interferograms for T_e=0.2-1.0keV. (c) Variations of fringe visibility ζ_T with the electron temperature for the quartz plate thickness=0.545, 0.550, 0.555mm.

birefringent plate in this design. The interferogram calculations take into account the wavelength-dependence of quartz birefringence and, for now, assume the spectrum to be ideally passed by the wideband filter. At a zero crossing, the scattered signals at the complementary output ports are

$$S_{\pm} = \frac{I_0}{2}\left[1 \pm \zeta_T(\phi_0)\right], \qquad (4)$$

where $\zeta_T(\phi_0)$ is the Thomson spectrum fringe visibility at delay $\phi_0 = M\pi$.

We concentrate to measure plasmas of $T_e <$ ~1keV in this study. This range corresponds to range of the electron temperature in TPE-RX as mentioned after. When the temperature exceeds 1 keV, the Thomson spectrum broadens and shifts to the blue due to the relativistic effect. However, it is the shift of the spectrum that most sensitively conveys the temperature, and this is registered by the interferogram as a phase change. Detailed discussion in case of the high temperature is described in Ref. 11.

Since proof-of-principle tests is carried out in TPE-RX using the existing YAG laser Thomson scattering system [13], parameters for design of a dual channel polarization interferometer are fixed as follows: $T_e \leq 1$ keV, $n_e \geq 5\times10^{19}$m^{-3}, scattering angle 90°, YAG laser wavelength 1064nm. The TPE-RX is a reversed-filed-pinch (RFP) machine at AIST, Japan (Major radius 1.72m, Minor radius 0.45m, plasma current 0.5MA, $T_e(0)$~1keV, pulse duration 100ms, shutdown in 2007). Thomson spectra and their associated interferograms for T_e = 0.2, 0.4, 0.6, 0.8, 1.0 keV are shown in Fig. 2(a), (b). To reject stray light of the YAG laser and reduce plasma background light, the wideband filter is placed at the entrance of the polarization interferometer. Variations of fringe visibility ζ_T with electron temperature for the quartz plate thickness = 0.545, 0.550, 0.555 mm are shown in Fig. 2(c).

Proof-of-principle tests of the polarization interferometer were carried out in TPE-RX. The pulsed poloidal current drive (PPCD) operation was applied to produce high T_e, n_e (T_e ~1keV, n_e ~1×10^{19}m^{-3}) plasmas. A YAG laser Thomson scattering system has been already installed in TPE-RX, and this system has a conventional filter polychromator (4 spectral channels). The existing Thomson scattering system is utilized for this test. The electron temperature of one spatial point at the plasma center was measured employing the filter polychromator and the polarization interferometer alternately. Typical waveforms of I_0, S_+ by Thomson scattering are shown in Fig.3(a), (b). To compare at different temperature ranges, data during PPCD (high temperature data) and before PPCD phase (low temperature) are measured as shown in Fig.3(c). Horizontal axis means shot number of the TPE-RX discharge in Fig.3(c). Average values using data

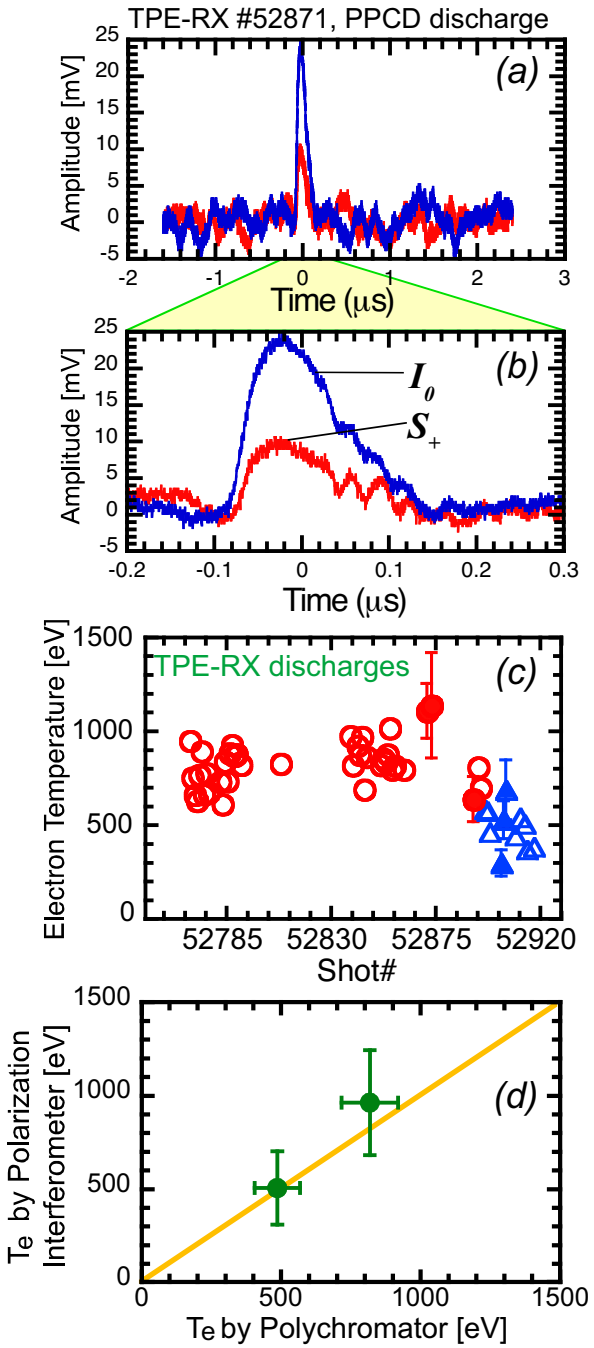

Fig.3 (a) Typical waveform of Thomson scattering signal using the dual channel polarization interferometer, and (b) its expansion of the time base. (c) T_e data by polychromator and the dual channel polarization interferometer. Horizontal axis means shot number of TPE-RX discharge. Circle and triangle symbols indicate data during PPCD (high temperature) and before PPCD (low temperature), respectively. Open and closed symbols indicate data from polychromator and polarization interferometer, respectively. (d) Comparison of T_e between polychromator and the dual channel polarization interferometer.

from Fig.3(d) are plotted for comparison between the polychromator and the polarization interferometer as shown in Fig.3(d). Similar T_e values within data variation and error bar ranges were measured by both spectrometers. The data variation of the polychromator is caused by reproducibility of the PPCD discharge and noise of detectors. The relatively large error of the polarization interferometer data proceeds from (1) entry of external noise to preamplifier circuit, (2) increasing of photon noise caused by increasing of intensity of background light (plasma light) due to Jacquinot and Fellgett advantages. To reduce the external noise, further shielding is necessary. To reduce the photon noise, it seems that appropriate filtering using bandpass filter is effective. In the polarization interferometer, T_e values around 1keV is higher than that of polychromator. Since the visibility curve as shown in Fig.2(c) is saturated around 1keV, it seems that the accuracy of the evaluation of T_e decreases.

3. Multichannel polarization interferometer

Measurement of one point on the interferogram using the dual channel polarization interferometer is insufficient to evaluate the electron temperature with the wider range. Although it is possible to evaluate the electron temperature with the wider range, several sets of the quartz plate of the different thickness are necessary in the dual channel polarization interferometer. We considered that measurement of the whole or the main part of interferogram is essential for the wider electron temperature range. When the whole or the main part of interferogram is measured, it is possible to reconstruct the Thomson scattered spectrum accurately. Various techniques for polarization interferometer have been proposed, so far [14]. A Wollaston prism [15,16] or a Savart plate [17,18] is used as typical techniques. A hybrid polarization interferometer employing a Wllaston prism with two Savart plate has been also proposed to make good use of the total incident light [19]. These techniques have been utilized for various applications: e.g. near infrared spectroscopy. We are developing a prototype multichannel polarization interferometer using the Wollaston prism to evaluate the availability for the Thomson scattering diagnostics.

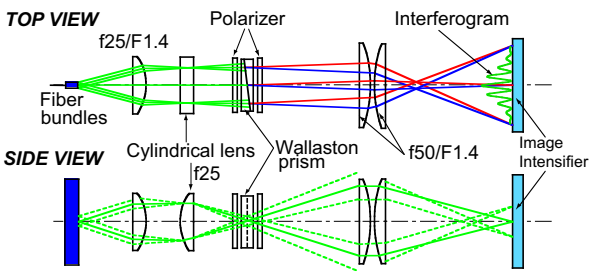

Fig.4 Optical diagram of the multichannel polarization interferometer using a Wollaston prism.

Figure 4 shows an optical diagram of the developing multichannel polarization interferometer. Bundled 102 optical fibers (cladding diameter = 200 μm, core diameter = 180 μm, numerical aperture = 0.3) are formed into a rectangular shape of 2.4mm x 1.6mm. One fiber bundle corresponds to one spatial channel. Several fiber bundles are used in this test. The light from the optical fiber bundles is collimated by a lens, and is introduced to an interferometer part. The interferometer part is simple structure that the Wollaston prism is sandwiched between two polarizers. By the first polarizer, the collimated beam is a linearly polarized at 45° to the optic axes of the Wallaston prism. The beam is divided into two orthogonally polarized beams with a separating angle by the Wollaston prism. The second 45° polarizer placed after the Wallaston prism permits the two orthogonal polarizations to interfere. An interferogram which is localized at a plane inside the Wallaston prism is imaged onto a photo cathode of an image intensified CCD camera by an imaging lens. In the case of the Thomson scattering measurement in JT-60U, existing the ruby laser Thomson scattering system [20] is utilized. The Wallaston prism with 22 by 22 mm square consists of quartz crystal. In the initial design, we selected following parameters: optical magnification M is 2 (1 at the final layout), the fringe frequency is 1 mm^{-1}, wavelength of ruby laser is 694.3nm.

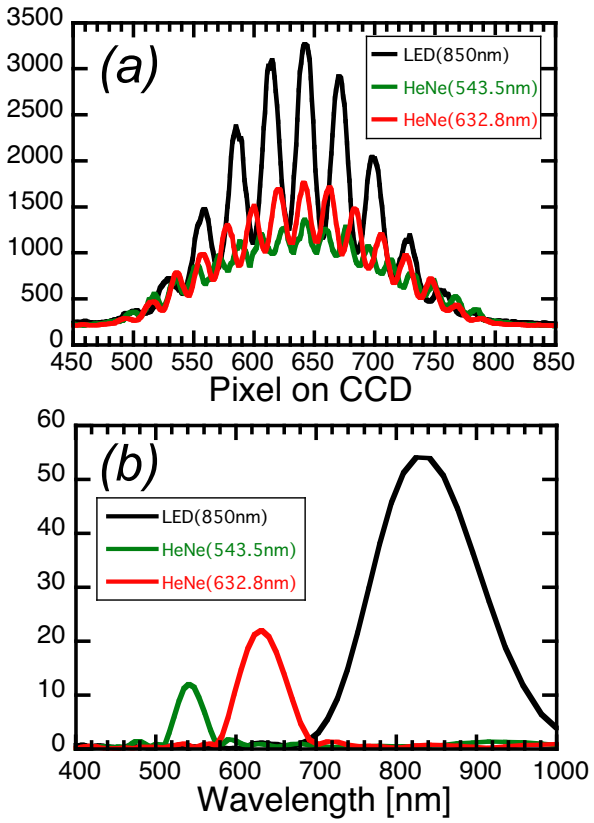

Fig.5 (a) Interferograms of LED(850nm), red He-Ne laser (632.8nm), green He-Ne laser (543.5nm), (b) their reconstructed spectra by Fourier transform.

Therefore, the apex angle and the separating angle of the Wallaston prism are 4° and 0.074°, respectively.

Interferograms of various monochromatic light sources were measured by the multichannel polarization interferometer as shown in Fig.5(a). In this test, a green He-Ne laser (λ=543.5nm), a red He-Ne laser (λ=632.8nm) and a near-infrared LED (λ=850nm) were used as light sources. Visibility of the interferogram is 0.44 in the case of 850-nm LED. The visibility decreases when the wavelength of the light source decreases. As one possibility, it seems that the relatively low visibility is caused by the aberration of the lenses. Figure 5(b) shows the Fourier transform (FFT) of interferograms shown in Fig.5(a), and original spectra of various light sources are reconstructed by FFT. Since 15-periods of the fringe can be observed for 632.8nm He-Ne laser in Fig.2(a), effective wavelength resolution becomes ~60nm in this system. It is possible to measure the electron temperature of more than 100 eV (scattering angle 90°) in this system. To measure low temperature of less than 100eV, it is necessary to increase the fringe frequency.

4. Conclusions

The polarization interferometer based on the Fourier transform spectroscopy for the Thomson scattering diagnostics has been developed to evaluate the validity. At the first stage, a dual channel polarization interferometer employing a fixed-thickness birefringent plate was developed to prove the principle of the Howard's method [11]. Proof-of-principle tests of the polarization interferometer were carried out in TPE-RX. Similar T_e values within data variation and error bar ranges were successfully measured by both the polarization interferometer and an existing filter polychroamtor. Therefore, the validity of the dual channel polarization interferometer was proved from this result. As the second stage, a multichannel polarization interferometer was developed to evaluate the availability for the Thomson scattering diagnostics. Interferograms of three kinds of monochromatic light sources were measured by the multichannel polarization interferometer, and those spectra was reconstructed by Fourier transform. It seems that the utilization of the multichannel polarization interferometer is promising for Thomson scattering diagnostics. As a future plan, we will conduct the electron temperature measurement by using the multichannel polarization interferometer for Thomson scattering diagnostics.

Acknowledgments

One of the authors (TH) wish to thank Drs. M. Kiyama, H. Sakakita, K. Yambe for their useful discussions at TPE-RX. This work is supported in part by Grant-in-Aid for Scientific Researches on Priority Area "Advanced diagnostics for burning plasma" from Ministry of Education, Culture, Sports, Science and Technology (No. 18035016, 20026011).

[1] N. J. Peacock, D. C. Robinson, M. J. Forrest, P. D. Wilcock, V. V. Sannikov, Nature **224**, 488 (1969).
[2] H. Yoshida, O. Naito, O. Yamashita *et al*., Rev. Sci. Instrum. **70**, 751 (1999).
[3] H. Röhr, K.-H. Steuer, H. Murmann, D. Meisel, IPP report III/121 B, July 1987.
[4] T. N. Carlstrom, G. L. Campbell, J. C. DeBoo, R. Evanko *et al*., Rev. Sci. Instrum. **63**, 4901 (1992).
[5] T. Hatae, A. Nagashima, T. Kondoh, S. Kitamura *et al*., Rev. Sci. Instrum. **70**, 772 (1999).
[6] K. D. Möller, *Optics* (University Science Books, Mill Valley, 1988) p.311.
[7] Fourier transform spectroscopy (July. 17, 2008, 10:08 UTC). In Wikipedia: The Free Encyclopedia. Retrieved from http://en.wikipedia.org/wiki/Fourier_transform_spectroscopy.
[8] J. Howard, C. Michael, F. Glass, and A. Cheetham, Rev. Sci. Instrum. **72**, (2001) 888.
[9] J. Howard, Appl. Otp. **41**, (2002) 197.
[10] J. Howard, C. Michael, F. Glass, and A. Danielsson, Plasma Phys. Control Fusion **45**, (2003) 1143.
[11] J. Howard, Plasma Phys. Control Fusion **48**, (2006) 777.
[12] T. Hatae, J. Howard, Y. Hirano, O. Naito, M. Nakatsuka, H. Yoshida, Plasma Fusion Res. **2**, S1026 (2007).
[13] H. Koguchi, Y. Hirano, H. Sakakita, et al., preprint of 21st IAEA Fusion Energy Conference, IAEA-CN-149/EX/P3-8 (2006).
[14] M. Françon, *Optical Interferometry* (Academic Press, New York, 1966) p.137.
[15] T. Okamoto, S. Kawata, S. Minami, Appl. Opt. **23**, 269 (1984).
[16] M. J. Padgett, A. R. Harvey, A. J. Duncan, W. Sibbett *et al*., Appl. Opt. **33**, 6035 (1994).
[17] M. Hashimoto, S. Kawata, Appl. Opt. **28**, 6096 (1992).
[18] C. Zhang, B. Xiangli, B. Zhao, X. Yuan, Optics Communications **203**, 21 (2002).
[19] N. Ebizuka, M. Wakaki, Y. Kobayashi, and S. Sato, Appl. Opt. **34**, 7899 (1995).
[20] H. Yoshida, O. Naito, O. Yamashita, S. Kitamura, T. Sakuma, Y. Onose, H. Nemoto, T. Hamano, T. Hatae, A. Nagashima, and T. Matoba, Rev. Sci. Instrum. **70**, 751 (1999).